HOMOGENIZATION MODELS FOR POLYMER-CLAY NANOCOMPOSITES: ONE- AND TWO-STEP APPRAOCHES

M. Pahalavpour[1], P. Hubert[2], M. Lévesque[1]*
[1] Mechanical Engineering Department, Ecole polyetechnique de Montreal, Montreal, Canada
[2] Mechanical Engineering Department, McGill University, Montreal, Canada
* Corresponding author (martin.levesque@polymtl.ca)

Keywords: *Homogenization, Finite Element, Nanocomposites, Nanoclay, Interphase*

1 Introduction

Polymer-Clay Nanocomposites (PCN) offer interesting applications to various sectors like packaging, transportation and construction. Fast and accurate predictive tools for behavior of such materials can highly accelerate their ever-growing applications by revealing their potential capacity.

Clays, in their natural form, have nano size thickness and lie parallely in stacks. Depending on the degree of separation and polymer penetration between the nano layers, three different morphologies for clay-polymer systems can be found: intercalated, exfoliated and aggregates. At molecular level, interactions at the interface between the nanoclay and polymer matrix result in the formation of an interphase with a thickness of a few nm.

Numerous studies have been performed on the analytical modeling of the both intercalated and exfoliated PCN [1–5]. However, only some have taken into account the interphase effects [4, 5]. The analytical studies can be generally categorized in one-step and two-step models. In two-step models, the two-phase composites models were used after homogenizing the reinforcing particles by an ”effective particle” concept [1, 2]. In ”effective particle” concept the layered particle (the exfoliated nanoclay surrounded by the interphase or the stack of intercalated particles) is homogenized in to a single phase. In one step models, which were mainly applied for the exfoliated nanoclays with or without interphase, all the presented phases (matrix and nanoclay and interphase) are models in one single step [4, 5].

However, no one-step study is yet performed for intercalated composites and more importantly, no comparative studies have been yet performed to compare the range of the validity, level of complexity and time-efficiency of two- and one-step models.
Numerical modeling of PCN has also been subject of numerous researches in last years. These models vary for simplified two-phase 2D Finite Element (FE) models [2–4, 6] to more complex 3D multiphase ones [6, 7]. In most of the numerical works, the representativeness of the analyzed models is not verified. Generally, these numerical studies have been used to validate the analytical models while their own exactitude is on question. The question may have roots in the effects of applied simplifications in the modeling on the overall results, namely, modeling the arranged particles (not randomly positioned), 2D modeling, applying simplified boundary conditions and not verifying the representativeness of the models.

In this work, the validity of some of commonly used analytical models, in both one-step and two-step categories were tested against 3D FE models of detailed microstructures. The Representative Volume Element (RVE) concept was used in FE modeling. The possible error introduced by different simplifying assumptions such as using two-step models and isotropy of particles, in both numerical and numerical models, was evaluated.

The paper is organized as follows: Section 2 presents a brief background on PCN and the modeling methods. Section 3 presents the proposed modeling strategy. The methodology adopted to conduct the comparative study is introduced in Section 4. Analysis of the results, experimental verification followed by the validation of homogenization models is carried out in Section 5.

2. background

2.1. PCN

Nanoclay platelets have a thickness of about 1 nm and their lateral dimensions may vary from 30 nm to several microns [8]. In exfoliated morphology, an interphase region forms around each nanoclay platelet (Fig. 1). In intercalated morphology, the interlayer space is called gallery and the distance between the central plane of the nanoclay and the corresponding plane in the next nanoclay sheet is referred by $d_{(001)}$. Since the thickness of each platelet is small, it was assumed that the interphase lied only on the nanoclay platelet top and bottom surfaces. Therefore, the thickness of the effective particle was obtained from:

$$d_{\mathrm{p}} = d_{\mathrm{s}} + 2d_{\mathrm{ı}} + (N-1)d_{(001)}, \tag{1}$$

where d refers to the thickness, subscripts s, p and ı refer to the silicate layer, the effective particle and the interphase, respectively and N denotes number of nanoclays in each stack.

2.2. Two-step homogenization models

Luo and Daniel [1], in a two-step model, considered intercalated PCN as two-phase composites by replacing the intercalated stacks of nanoclays by an equivalent homogenized particle. Equivalent homogenized particles were also used by Sheng et al. [2] and were named "effective particles". This concept was then used by other researches for both intercalated and exfoliated nanocomposites [2–4, 9].

2.3. First step

In work of Mesbah et al. [4] and Pahlavanpour et al. [9] the properties of the effective particles (Young's modulus (E), Poissoin's ratio (ν) and shear modulus (G)) were computed as per the modified rule of mixtures by Tsai and Hahn [10] as:

$$E_{\mathrm{p},11} = E_{\mathrm{p},33} = \chi E_{\mathrm{s}} + (1-\chi)E_{\mathrm{t}}, \tag{2}$$

$$\nu_{\mathrm{p},12} = \nu_{\mathrm{p},32} = \chi \nu_{\mathrm{t}} + (1-\chi)\nu_{\mathrm{s}}, \tag{3}$$

$$E_{\mathrm{p},22} = \frac{E_{\mathrm{s}}E_{\mathrm{t}}}{\chi E_{\mathrm{t}} + (1-\chi)E_{\mathrm{s}} - \chi(1-\chi)\beta E_{\mathrm{t}}E_{\mathrm{s}}}, \tag{4}$$

$$\nu_{\mathrm{p},13} = \frac{\chi\nu_{\mathrm{s}}E_{\mathrm{s}}(1-\nu_{\mathrm{t}}^2) + (1-\chi)\nu_{\mathrm{t}}E_{\mathrm{t}}(1-\nu_{\mathrm{s}}^2)}{\chi E_{\mathrm{s}}(1-\nu_{\mathrm{t}}^2) + (1-\chi)\nu_{\mathrm{t}}E_{\mathrm{t}}(1-\nu_{\mathrm{s}}^2)}, \tag{5}$$

$$G_{\mathrm{p},12} = G_{\mathrm{p},32} = \frac{G_{\mathrm{s}}G_{\mathrm{t}}}{\chi G_{\mathrm{t}} + (1-\chi)G_{\mathrm{s}} - \chi(1-\chi)\eta G_{\mathrm{t}}G_{\mathrm{s}}}, \tag{6}$$

$$G_{\mathrm{p},13} = \frac{E_{\mathrm{p},11}}{2(1+\nu_{\mathrm{p},13})}, \tag{7}$$

where subscripts 1, 2 and 3 correspond to the principal axes shown in Fig. 2. Subscripts m, p and t, refer to matrix/bulk polymer, effective particle and the third phase (interphase or gallery) respectively. χ is the silicate volume fraction in the effective particle, defined as:

$$\chi = \frac{N\,d_{\mathrm{s}}}{d_{\mathrm{p}}}. \tag{8}$$

β and η are defined as:

$$\beta = \frac{\nu_{\mathrm{s}}^2 E_{\mathrm{t}}/E_{\mathrm{s}} + \nu_{\mathrm{t}}^2 E_{\mathrm{s}}/E_{\mathrm{t}} - 2\nu_{\mathrm{s}}\nu_{\mathrm{t}}}{\chi E_{\mathrm{s}} + (1-\chi)E_{\mathrm{t}}},$$
$$\eta = \frac{\nu_{\mathrm{s}}^2 G_{\mathrm{t}}/G_{\mathrm{s}} + \nu_{\mathrm{t}}^2 G_{\mathrm{s}}/G_{\mathrm{t}} - 2\nu_{\mathrm{s}}\nu_{\mathrm{t}}}{\chi G_{\mathrm{s}} + (1-\chi)G_{\mathrm{t}}}. \tag{9}$$

The relationship between the volume fraction of the effective particle, f_{p}, and the volume fraction of the silicate phase in the composite, f_{s} is:

$$f_{\mathrm{p}} = \frac{f_s}{\chi}. \tag{10}$$

The aspect ratio of the effective particle, a_{p}, was defined as

$$a_{\mathrm{p}} = \frac{d_{\mathrm{p}}}{\ell}, \tag{11}$$

where ℓ is the length of the nanoclay platelet. Eqs (2-7) present the properties of the Transverse Isotropic (TIso) Effective Particle (EP). For the simplified Isotropic (Iso) EP, only two independent constants, E_{p} and ν_{p}, were required, which were approximated by $E_{p,11}$ and $\nu_{p,12}$ (Eqs. (2) and (3), respectively).

2.4. Second step

Both analytical and numerical micromechanical models can be subsequently used in a second step to calculate the mechanical properties of the nanocomposite [1–4, 9]. Pahlavanpour et al. [9] performed an evaluation study on the validity of some of commonly used micromechanical models for the prediction of exfoliated PCN's elastic properties against results of 3D periodic FE simulations. They found that the MT model is the most reliable method to be used as the second homogenization step for all possible ranges of modulus contrast, aspect ratio of reinforcing phase and its volume fraction in exfoliated PCN.

2.5. One-step analytical homogenization models

Two one-step analytical models used in this paper are the models developed for predicting the properties of composites with coated particles. One is based on double-inclusion [11] model that deals with particle with single layer of coating and the other treats composites containing particles with multilayer coating [12].

The double-inclusion model as proposed by Hori and Nemat-Nasser [11] deals with a composite inclusion consists of an ellipsoidal inclusion embedded in another ellipsoidal coating layer, that is, further embedded in an infinitely extended homogeneous medium. The shape and orientation of the inclusion and the coating, and the elastic properties of the three phases can be arbitrary. Ju and Chen [13] derived the general governing equations for composites containing unidirectionally oriented particles, called "Interacting Double Inclusion" (IDI) approach herein. This approach is used in order to take into account not only the particle-matrix interaction, but also the interaction between particles. In the case of three-phase nanocomposites, and according to Liu and Sun [14], one may write the effective stiffness tensor of the nanocomposite, $\mathbf{C}^{\text{eff}}$, as

$$\mathbf{C}^{\text{eff}} = \mathbf{C}^0 : [\mathbf{I} - \Phi_\Sigma \mathbf{T}^\Sigma : (\Phi_\Sigma \mathbf{S}^\Sigma + \mathbf{I})^{-1}], \qquad (12)$$

where $\mathbf{C}^0$ denotes the stiffness tensor of the matrix, $\mathbf{I}$ refers to the fourth-order identity tensor, Φ_Σ is the volume fraction of composite inclusion and $\mathbf{T}^\Sigma$ is the fourth-order tensor given by:

$$\mathbf{T}^\Sigma = \phi_{\text{p}} \mathbf{T}^{\text{p}} + \phi_{\text{i}} \mathbf{T}^{\text{i}}. \qquad (13)$$

$\mathbf{T}^{\text{p}}$ and $\mathbf{T}^{\text{i}}$ are two fourth-order tensors defined by

$$\mathbf{T}^{\text{p}} = -[(\mathbf{S}^{\text{p}} + \mathbf{A}^{\text{p}}) + \Delta\mathbf{S} : \left(\mathbf{S}^{\text{p}} - \phi_{\text{p}}/\phi_{\text{i}} \Delta\mathbf{S} + \mathbf{A}^{\text{i}}\right)^{-1} : \left(\mathbf{S}^{\text{p}} - \phi_{\text{p}}/\phi_{\text{i}} \Delta\mathbf{S} + \mathbf{A}^{\text{p}}\right)]^{-1}, \qquad (14)$$

$$\mathbf{T}^{\text{i}} = -[\Delta\mathbf{S} + (\mathbf{S}^{\text{p}} + \mathbf{A}^{\text{p}}) : \left(\mathbf{S}^{\text{p}} - \phi_{\text{p}}/\phi_{\text{i}} \Delta\mathbf{S} + \mathbf{A}^{\text{p}}\right)^{-1} : \left(\mathbf{S}^{\text{p}} - \phi_{\text{p}}/\phi_{\text{i}} \Delta\mathbf{S} + \mathbf{A}^{\text{i}}\right)]^{-1}, \qquad (15)$$

where ϕ_{p} and ϕ_{i} refer to the particle and interphase volume fraction inside the composite inclusion $\Sigma = \text{p} + \text{i}$, $\Delta\mathbf{S}$ denotes $\mathbf{S}^\Sigma - \mathbf{S}^{\text{p}}$ where $\mathbf{S}$ are the Eshelby tensors [15] for the composite inclusion medium Σ and the particle p, respectively. These tensors only depend on the Poisson's ratio of the matrix and on the aspect ratio of the medium. A^{p} and A^{i} are two mismatch material property fourth-order tensors for domain p and i expressed by

$$\mathbf{A}^{\text{p}} = (\mathbf{C}^{\text{p}} - \mathbf{C}^0)^{-1} : \mathbf{C}^0, \qquad \mathbf{A}^{\text{i}} = (\mathbf{C}^{\text{i}} - \mathbf{C}^0)^{-1} : \mathbf{C}^0. \qquad (16)$$

In a simplified version of this model, called simplified IDI hereinafter, it is assumed that the interphase around the particle has the same aspect ratio as that of the particle: $\mathbf{S}^\Sigma = \mathbf{S}^{\text{p}}$ and $\Delta\mathbf{S} = 0$. Consequently, Eqs. (14) and (15) become much simpler. Mesbah et al. [4] used simplified IDI to predict the elastic properties of exfoliated PCN.

A one-step model to deal with linear elastic n-layered coated ellipsoids is the model of Lipinski et al. [12], called "multi-coated model" hereinafter. The model is a self-consistent model based on a combination of Greens function techniques with interface operators, illustrating the stress and strain jump conditions at the interfaces between two adjacent coatings, which are considered perfectly bonded. In this model, the stiffness tensor of the composite is calculated as:

$$\mathbf{C}^{\text{eff}} = \mathbf{C}^0 + \sum_{j=1}^{n} \phi_j (\mathbf{C}^j - \mathbf{C}^0) : \mathbf{A}^{(j)}, \qquad (17)$$

where the strain concentration tensors $\mathbf{A}^{(j)}$ [12], determinated by the Generalized Self-Consistent Scheme (GSCS), takes the form $\mathbf{A}^{(j)} = \alpha^j : A$ where

$$\mathbf{A} = \left[\mathbf{I} + \mathbf{T}^{\text{I}}(\mathbf{C}) : \left(\sum_{j=0}^{n} \phi_j \Delta\mathbf{C}^{(j/\text{eff})} : \boldsymbol{\alpha}^j\right)\right]^{-1}, \qquad (18)$$

and $\Delta\mathbf{C}^{(j/\text{eff})} = \mathbf{C}^j - \mathbf{C}^{\text{eff}}$ [12]. The concentration operators $\boldsymbol{\alpha}^j$ are

$$\boldsymbol{\alpha}^1 = \left(\sum_{j=0}^{n} \phi_j \mathbf{w}^j\right)^{-1}, \qquad (19)$$

$$\boldsymbol{\alpha}^j + 1 = \mathbf{w}^j + 1 : \boldsymbol{\alpha}^1,$$

where the tensor $\mathbf{w}^i$ is defined such that

$$\mathbf{w}^1 = \mathbf{I}, \quad \mathbf{w}^2 = \boldsymbol{\omega}^{(2/1)}, \qquad (20)$$

$$\mathbf{w}^{j+1} = \frac{\sum_{k=1}^{j} \left(\phi_k \boldsymbol{\omega}^{(j+1/k)} : \mathbf{w}^k\right)}{\sum_{k=1}^{j} \phi_k}.$$

$\boldsymbol{\omega}^{(j+1/k)}$ is the concentration tensor describing the jump of average strains between the layer $j+1$ and layer k. The expressions below defines the general form of this tensor

$$\boldsymbol{\omega}^{(j+1/k)} = \mathbf{I} - \left[\mathbf{T}^{\Omega_j}(\mathbf{C}^{j+1}) - \frac{\sum_{l=1}^{j} \phi_l}{\phi_{j+1}} (\mathbf{T}^{\Omega_{j+1}}(\mathbf{C}^{j+1}) - \mathbf{T}^{\Omega_j}(\mathbf{C}^{j+1}))\right] : \Delta\mathbf{C}^{(j+1/k)} \quad \text{for} \quad k = 1, .., j \qquad (21)$$

where $\Delta\mathbf{C}^{(j+1/k)} = \mathbf{C}^{j+1} - \mathbf{C}^{k}$ and

$$\mathbf{T}^{\Omega_{j+1}}(\mathbf{C}^{j+1}) = \mathbf{S}^{\Omega_{j+1}}(\mathbf{C}^{j+1}) : (\mathbf{C}^{j+1})^{-1}, \qquad (22)$$

in which $\mathbf{S}^{\Omega_{j+1}}(\mathbf{C}^{j+1})$ is the well-known Eshelby tensor which depends on aspect ratio of the inclusion Ω_{j+1} and matrix $\mathbf{C}^{j+1}$ elastic properties.

3. The modeling strategy

The multiscale modeling strategy used herein consisted of both two-step and one-step homogenizations. In two-step models, step I aimed at computing the effective properties of the stack of nanoclay platelet surrounded by its interface. This allowed computing the EP properties. The effective particles were then considered as inclusions in Step II where different analytical models (i.e. Mori-Tanaka (MT) model [16, 17], Lielens's model [18] and Self-Consistent (SC) scheme [19, 20]), as well as numerical homogenization models were used to obtain the overall properties. Employing different analytical models as the second step combined with the EP concept as the first step of homogenization lead to the different analytical modeling procedures (i.e. MT/EP, Lielens/EP and SC/EP).

In one-step models, both IDI and multi-coated models are used for exfoliated morphologies. For the intercalated morphology, the multi-layer stack is modeled as a multi-coated ellipsoid. Considering the very small thickness of the nanoclay and its high aspect ratio in this morphology (0.005), this assumption seems to be reasonable.

In numerical modeling, Layered Particles (LP) are modeled as well as the EP following the same methodology explained in [9]. Randomly distributed aligned disk-shaped particles were generated in 3D periodic Volume Elements (VE) using an algorithm based on Molecular Dynamics simulations [9, 21]. Periodic boundary conditions were enforced. The Representative Volume Element (RVE) concept is used following the procedure explained by Pahlavanpour et al. [9] through a two-fold convergence study.

The assumption in both numerical and analytical models is that all the constituent phases are linearly elastic and perfectly bonded at their interface.

4. Methodology for quantitative analyses

The properties of the silicate layers were taken from the results of computational chemistry simulations available in the literature [22]. The relation to convert the nanoclay weight fraction, w_s, to its volume fraction, f_s, is linearized as [2]

$$f_s \approx \frac{\rho_m}{\rho_s}\frac{1}{\psi}w_s, \qquad (23)$$

where ρ is the density of each phase and subscript m refers to the matrix and

$$\psi = \frac{1}{\left(1-\frac{1}{N}\right)\left(\frac{d_{(001)}}{d_s}\right)+\frac{1}{N}}. \qquad (24)$$

A density value of $\rho_m = 1000\ kgm^{-3}$ was assigned to the matrix [2]. The density of clay platelets, according to Chen et al. [22] was considered as $3067\ kgm^{-3}$.

4.1. Exfoliated morphology

The properties of constituent phases are listed in Table 1. For comparison purposes, another case with an imaginary interphase, Case II, is also introduced in Table 1. In the lower part of the Table 1, the EP properties obtained form the first step of homogenization are presented for both Cases.

For experimental validation, experimental data on Nylon-6/MMT nanocomposites by Fornes et al. [23] was used. They claimed nearly complete exfoliation and good particle alignment with clay content varying from 1.6 to 7.2 wt% [23].

4.2. Intercalated morphology

Constituent phases of the intercalated morphology are presented in Table 2. The lower part of the Table 2 presents the properties of the EP calculated from the first step of homogenization.

For experimental validation, experimental data on MXD6 Nylon/MMT nanocomposites by Sheng et al. [2], with clay content varying from 1.1 to 5.27 wt%, was used. Intercalated multi-layer stacks were observed to be well aligned and the structure of intercalated clay stacks is independent of clay content; in particular, the average N is 3; and the average interlayer space, $d_{(001)}$ is 4.1 nm [2].

5. Results and discussion

5.1. Numerical models : Error induced by two-step models

A simple case that may clearly reveal the possible errors induced by two-step models is the case of exfoliated morphology with imaginary interphase, Case II in Table 1. Fig. 3 shows the numerical results for Case II

with both two-step and one-step methods. Although results of these two methods should be theoretically the same, using Iso EP at nanoclay volume fraction of 4% leads to 13% of overestimation of axial Young's modulus E_{11} compared to one-step model with real layered particles. It is shown that although using the TIso EP can slightly reduce the error, the overestimation is still up to 10%. In Fig. 4, the effect of EP concept is investigated for an exfoliated PCN with real interphase. The overestimation of the Iso EP is up to 5% whereas use of the TIso EP can reduce this value to 3.5%. The effect of using EP concept on the predictions for intercalated morphologies is shown in Fig. 5, where the Iso EP has an error of 3% compared to one-step method with real LPs. Data analysis of the errors occurred in two-step models, Figs. 3-5, reveals that volume fraction of nanoclay (f_s), rigidity contrast between nanoclay and EP (E_s/E_p) and inverse of their aspect ratios (a_p/a_s) have direct relationship with the percentage error induced by EP concept. In other word, the more the EP is different form the nanoclay, in terms of rigidity and aspect ratio, the more the error of two-step models is pronounced. Table 3 lists the the influence of rigidity contrast and aspect ratio for the three studied cases at fix volume fraction.

One-step numerical models are computationally more costly than the two-step models in terms of computation memory and time. In the studied cases, the number of elements was considerably increased (> 5 *times*) in models with LP compared to the model consisted of EP. Given the much lower computational cost of two-step numerical models, one may conclude that the error induced by EP concept can be acceptable depending on the application of the results. However, when it comes to set the numerical results as the benchmark to validate the analytical models, any initial error reduces the exactitude of the evaluation.

5.2. Experimental validation

To verify the general validity of layered numerical models, experimental data were compared to those of numerical simulations for both intercalated and exfoliated morphologies in Figs. 6 and 7. It is shown that the numerical models are very well able to reproduce the experimental results, especially in exfoliated morphology.

5.3. Analytical models

For the exfoliated morphology, the analytical results obtained by different models are compared to those of numerical simulations. It is shown that IDI simplified model delivers result with large errors. The best analytical model is the one-step IDI model that reproduces numerical results with slightly more accuracy than those of the two-step MT/TIso EP model and the one-step multi-coated model.

For the intercalated case, the best analytical model is the one-step multi-coated that reproduce the numerical results with less than 1% error. The MT/Iso EP model very well follows its corresponding numerical model, FE-Iso EP, but it delivers results with 4% error compared to one-step FE-LP results. The one-step IDI models are not applicable for intercalated morphology because of its multilayer structure. The SC model clearly overestimates the axial Young's modulus. Although the rigidity contrast between the EP and the matrix is high (≈ 15), the Lielens' model does not improve on MT model probably because of law volume fraction of the EPs (< 7%) [9]. Considering higher computational cost of the multi-coated model and being more difficult to be implemented, one may conclude that the MT model is the most viable analytical model to predict axial Young's modulus of intercalated PCN. However, it is recommended to use the multi-coated model to predict intercalated morphologies with high volume fractions or high contrasts of rigidity.

6. Conclusions

This work evaluated both two-step and one-step analytical models using 3D FE models of detailed representative microstructures. The possible error introduced by two-step models in both numerical and analytical models, was evaluated. The RVE concept was also used in FE modeling. This study covered both intercalated and exfoliated morphologies. Experimental verification with data extracted from the literature was also used to validate the overall numerical modeling. Numerical simulations revealed that using two-step models, relying on effective particle concept, may introduce considerable percentage of error (up to 13% in the studied cases). It was found that the more the effective particle is different form the nanoclay, in terms of rigidity and aspect ratio, or the higher the volume fraction is, the more the error of two-step models is pronounced. Given the much lower computational cost of two-step numerical models, the error induced by EP concept can be acceptable depending on the application of the results. However, when the numerical simulations are to be used as validating means whose accuracy should be unquestionable, the one-step models are recommended.

In analytical modeling, the two-step MT/EP model generates very well the exfoliated results whereas in in-

tercalated morphologies, it delivers predictions with a low percentage error ($< 4\%$) compared to one-step numerical model. IDI model followed by multi-coated model is found to be the most accurate one-step analytical model for exfoliated morphology. For the intercalated morphology, the multi-coated model is the only model that delivers very accurate results. Given the less computational cost and simplicity of two-step MT-based models, this model is recommended viable to be exploited as a fast and reliable analytical model. However, it is recommended to use the multi-coated model to predict intercalated morphologies with high volume fractions or high contrasts of rigidity.

7. Acknowledgments

This research was funded by the National Research Council Canada under NRC-NSERC-BDC Initiative program on "Polyester Nanocomposites for Greener Transportation, Construction and Packaging Applications" project.

References

[1] J.-J. Luo, I. M. Daniel, Characterization and modeling of mechanical behavior of polymer/clay nanocomposites, Composites Science and Technology 63 (2003) 1607 – 1616.

[2] N. Sheng, M. C. Boycea, D. M. Parks, G. C. Rutledgeb, J. I. Abesb, R. E. Cohen, Multiscale micromechanical modeling of polymer/clay nanocomposites and the effective clay particle, Polymer 45 (2004) 487–506.

[3] L. Figiel, C. P. Buckley, Elastic constants for an intercalated layered-silicate/polymer nanocomposite using the effective particle concept - a parametric study using numerical and analytical continuum approaches, Computational Materials Science 44 (2009) 1332 – 1343.

[4] A. Mesbah, F. Zaïri, S. Boutaleb, J. M. Glaoguen, M. Naït-Abdelaziz, S. Xie, T. Boukharouba, J. M. Lefebvre, Experimental characterization and modeling stiffness of polymer/clay nanocomposites within a hierarchical multiscale framework, Journal of Applied Polymer Science (2009) 3274–3291.

[5] K. Anoukou, F. Zaïri, M. Naït-Abdelaziz, A. Zaoui, T. Messager, J. Gloaguen, On the overall elastic moduli of polymer–clay nanocomposite materials using a self-consistent approach. part i: Theory, Composites Science and Technology 71 (2011) 197–205.

[6] K. Hbaieb, Q. Wang, Y. Chia, B. Cotterell, Modelling stiffness of polymer/clay nanocomposites, Polymer 48 (2007) 901 – 909.

[7] G. Cricri, E. Garofalo, F. Naddeo, L. Incarnato, Stiffness constants prediction of nanocomposites using a periodic 3d-fem model, Journal of Polymer Science Part B: Polymer Physics 50 (2011) 207–220.

[8] S. S. Ray, M. Okamoto, Polymer/layered silicate nanocomposites: a review from preparation to processing, Progress in Polymer Science 28 (2003) 1539 – 1641.

[9] M. Pahlavanpour, H. Moussaddy, E. Ghossein, P. Hubert, M. Lévesque, Prediction of elastic properties in polymer-clay nanocomposites: Analytical homogenization methods and 3d finite element modeling, Computational Materials Science (Submitted on January 2012).

[10] S. W. Tsai, H. T. Hahn, Introduction to Composite Materials, Technomic Pub.: Lancaster, Pennsylvania, USA, 1980.

[11] M. Hori, S. Nemat-Nasser, Double-inclusion model and overall moduli of multi-phase composites, Mechanics of materials 14 (1993) 189–206.

[12] P. Lipinski, E. H. Barhdadi, M. Cherkaoui, Micromechanical modelling of an arbitrary ellipsoidal multi-coated inclusion, Philosophical Magazine 86 (2006) 1305–1326.

[13] J. W. Ju, T. M. Chen, Micromechanics and effective moduli of elastic composites containing randomly dispersed ellipsoidal inhomogeneities, Acta Mechanica 103 (1994) 103–121.

[14] H. Liu, L. Sun, Multi-scale modeling of elastoplastic deformation and strengthening mechanisms in aluminum-based amorphous nanocomposites, Acta Materialia 53 (2005) 2693–2701.

[15] J. D. Eshelby, The determination of the elastic field of an ellipsoidal inclusion, and related problems, Proceedings of the Royal Society of London A 241 (1957) 376–396.

[16] T. Mori, K. Tanaka, Average stress in matrix and average elastic energy of materials with misfitting inclusions, Acta metallurgica 21 (1973) 571–574.

[17] Y. Benveniste, A new approach to the application of mori-tanaka's theory in composite materials, Mechanics of Materials 6 (1987) 147–157.

[18] G. Lielens, Micro-Macro Modeling of Structured Materials, Ph.D. thesis, Universite Catholique de Louvain, 1999.

[19] R. Hill, A self-consitent mechanics of composites materials, J. Mech. Phys. Solids 13 (1965) 213–222.

[20] B. Budiansky, On the elastic moduli of some heterogeneous materials, Journal of the Mechanics and Physics of Solids 13 (1965) 223–227.

[21] E. Ghossein, M. Lévesque, A fully automated numerical tool for a comprehensive validation of homogenization models and its application to spherical particles reinforced composites, International Journal of Solids and Structures 49 (2012) 1387–1398.

[22] B. Chen, J. R. G. Evansand, H. C. Greenwell, P. Boulet, P. V. Coveney, A. A. Bowdenf, A. Whiting, A critical appraisal of polymer–clay nanocomposites, Chemical Society Reviews 37 (2008) 568–594.

[23] T. D. Fornes, P. J. Yoon, H. Keskkula, D. R. Paul, Nylon 6 nanocomposites: the effect of matrix molecular weight, Polymer 42 (2001) 9929–9940.

[24] W. Xu, Q. Zeng, A. Yu, Young's modulus of effective clay clusters in polymer nanocomposites, Polymer 53 (2012) 3735–3740.

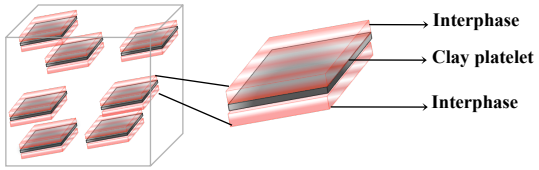

Figure 1: Three-layer reinforcing stacks in exfoliated composites.

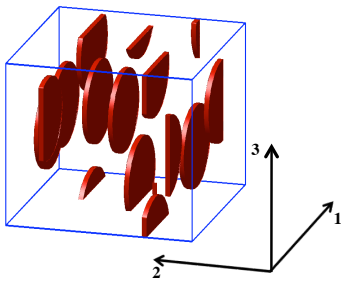

Figure 2: Periodic volume element with disk-shaped particles aligned perpendicular to the axis 2.

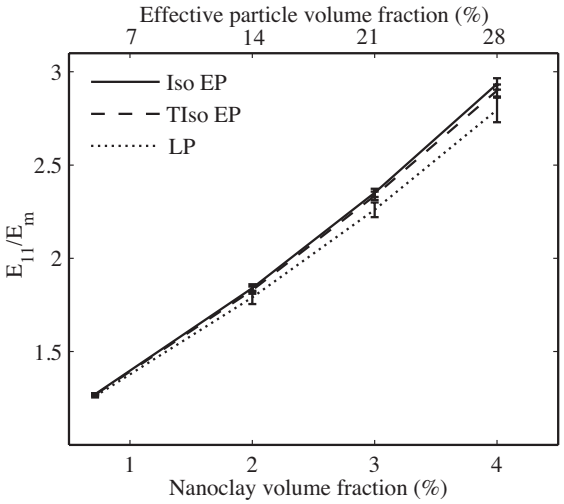

Figure 4: Prediction of one-step (LP) and two-step (Iso EP and Tiso EP) FE models for exfoliated morphology with the real interphase, Case I. The bars correspond to confidence intervals on the average level of 95%.

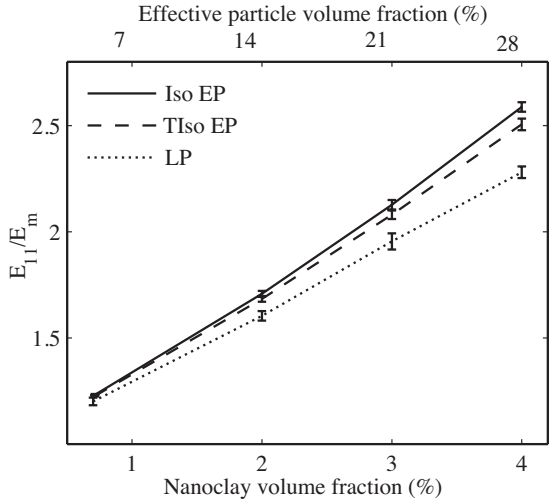

Figure 3: Prediction of one-step (LP) and two-step (Iso EP and Tiso EP) FE models for exfoliated morphology with the imaginary interphase, Case II. The bars correspond to confidence intervals on the average level of 95%.

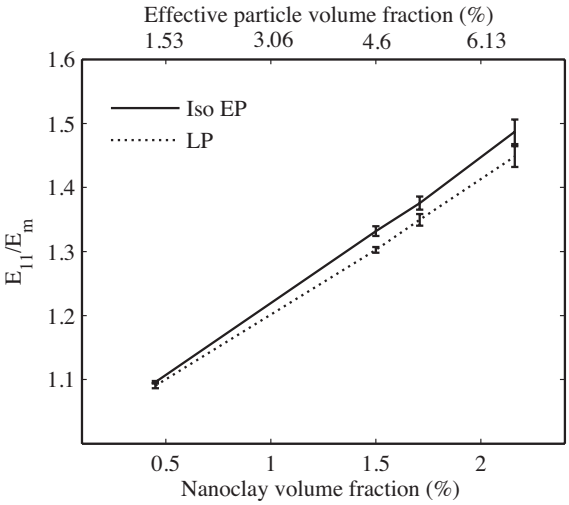

Figure 5: Prediction of one-step (LP) and two-step (Iso EP) FE models for intercalated morphology. The bars correspond to confidence intervals on the average level of 95%.

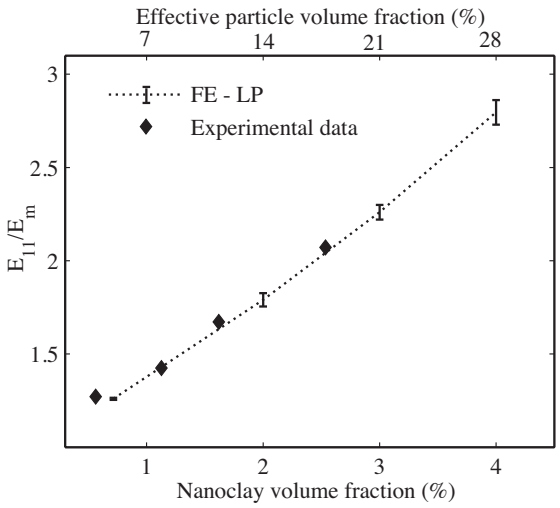

Figure 6: Experimental validation of one-step (LP) FE model for exfoliated morphology, Case I. The bars correspond to confidence intervals on the average level of 95%.

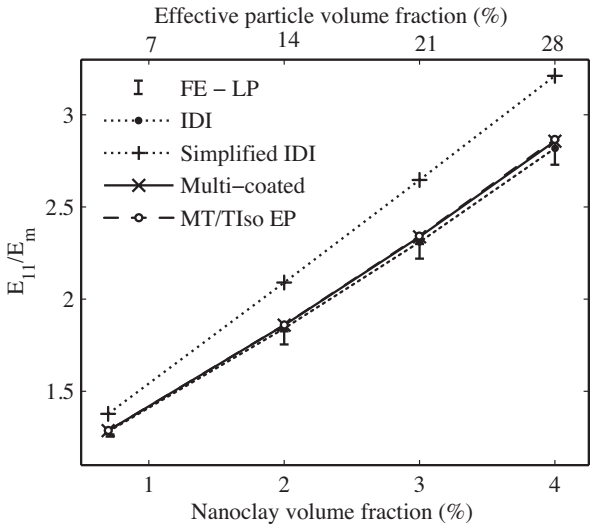

Figure 8: Validation of one-step (Multi-coated, IDI, simplified IDI) and two-step (MT/TIso EP) analytical models against one-step (LP) FE model. Exfoliated morphology, Case I. The bars correspond to confidence intervals on the average level of 95%.

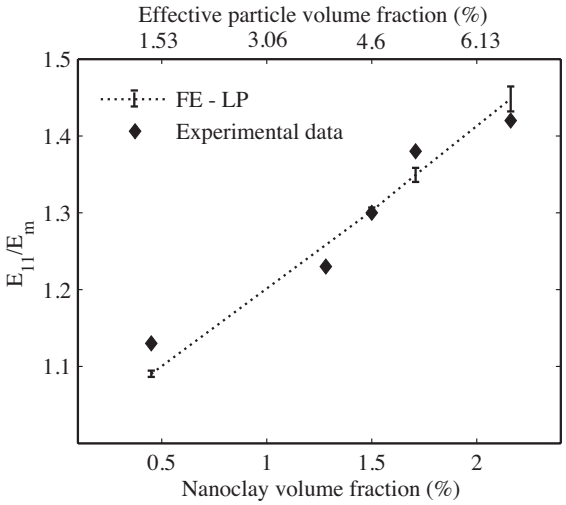

Figure 7: Experimental validation of one-step (LP) FE model for intercalated morphology. The bars correspond to confidence intervals on the average level of 95%.

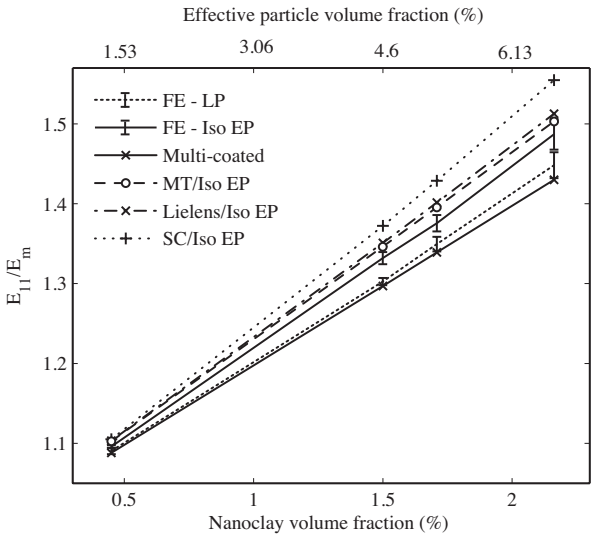

Figure 9: Validation of one-step (Multi-coated) and two-step (MT/Iso EP, Lielens's/Iso EP, SC/Iso EP) analytical models against one-step (LP) FE model. Intercalated morphology. The bars correspond to confidence intervals on the average level of 95%. analytical models, intercalated case.

Table 1: Property of phases in the exfoliated PCN.

			Young's modulus E (GPa)	Poisson ratio ν	Thickness d (nm)
Matrix (Nylon-6) [23]			2.8	0.35	NA
Nanoclay (MMT) [22]			178	0.28	1*
Interphase	Case I [9, 24]		13	0.35	3
	Case II		2.8	0.35	3
Effective Particle	Case I	Iso	36.6	0.34	7
		TIso	$E_{11} = E_{33} = 36.6$ $E_{22} = 16.2$ $(G_{12} = G_{32} = 6.01,$	$\nu_{12} = \nu_{32} = 0.34$ $\nu_{13} = 0.37$ $G_{13} = 13.25$ GPa)	7
	Case II	Iso	27.82	0.34	7
		TIso	$E_{11} = E_{33} = 27.82$ $E_{22} = 3.65$ $(G_{12} = G_{32} = 1.35,$	$\nu_{12} = \nu_{32} = 0.34$ $\nu_{13} = 0.3$ $G_{13} = 10.66$ GPa)	7

* Nanoclay aspect ratio was considered as 0.01 in all exfoliated configurations.

Table 2: Property of phases in the intercalated PCN.

	Young's modulus E (GPa)	Poisson's ratio ν	Isotropy	Thickness d (nm)
Matrix (MXD6 Nylon)	4.14	0.35	Iso	NA
Nanoclay (MMT) [22]	178	0.28	Iso	1*
Gallery [2]	4.14	0.35	Cubic symmetry ($G = 0.015$ GPa)	3.1
Effective Particle	60.83	0.33	Iso	9.2

* Nanoclay aspect ratio was considered as 0.005.

Table 3: Influence of rigidity contrast and aspect ratio in error induced by two-step numerical models.

	E_s/E_p	a_p/a_s	Error*
Intercalated PCN	2.93	9.2	2.18%
Exfoliated (Case I)	4.86	7	2.82%
Exfoliated (Case II)	6.4	7	6.47%

* The error is calculated between the Iso EP and LP models.
$f_s = 2\%$ for all the three cases.